Airfoil noise reduction by serrations and/or tubercles and model-to-full scale noise transposition
PIBE Project report, Work Package 3

Michel Roger
École Centrale de Lyon, LMFA, Ecully, France,

Benjamin Cotté
ENSTA Paris, IMSIA, Palaiseau, France

June 1, 2024

Contents

Abstract

This document reports about two aspects of the project activity in work-package 3. The first one is the assessment of trailing-edge serrations and leading-edge tubercles as mitigation devices, from aeroacoustic wind-tunnel tests in both static and dynamic conditions. The second one is about general issues in the transposition of model-scale results to full scale.

Chapter 1

Preliminary Considerations on the Effects of Serrations and Model-to Full Scale Transposition

1 Introduction

Trailing-edge (TE) serrations, on the one hand, and leading-edge (LE) serrations, more appropriately referred to as tubercles or wavy shape for thick and rounded leading edges, on the other hand, are recognized as mitigation means for the broadband and/or tonal noise of airfoils. Their performances in terms of noise reduction have been reported in many research studies, based either on tests performed in anechoic facilities, refined numerical simulations or dedicated analytical models. Yet the effect of leading-edge and trailing-edge devices is only described in the literature for steady-state flow conditions. This motivated the present investigation of the dynamic stall regime, in the work package 3 of PIBE. Both technologies are assessed on a NACA-$63_3$418 airfoil, comparing with the static conditions taken as reference and the straight-edge airfoil as baseline.

A recent bibliographical survey on LE and TE modifications as bio-inspired devices is found, for instance, in [19].

2 Trailing-Edge Serrations

Trailing-edge serrations are often presented as a device inspired by the fringes on the wings of owls, the silent flight of which is a well-known fact [19]. They reduce the trailing-edge noise associated with attached turbulent boundary layers. Many shapes of the serrations, including multiple wavelengths, random shapes and tooth profiles, have been considered. In the present work, only the triangular cut is addressed, as more representative of existing wind-turbine applications [13]. Reported observations in wind-tunnel experiments suggest that the best performing triangular cuts are with a quite large edge angle and a spanwise wavelength of the same order of magnitude as the boundary-layer thickness. For instance, tests performed on a linear cascade of lifting airfoils by Finez *et al* [10] with serrations of wavelength and depth 2 mm and 7 mm, for a chord length of 10 m and an estimated boundary-layer thickness of about 4-to-5 mm, achieved significant noise reductions of 3-4 dB in an extended frequency range. The effectiveness on wind turbines has also been demonstrated [14, 13], leading to increasingly systematic implementation as addons on existing large wind turbines or as initial design parts at the stage of manufacturing.

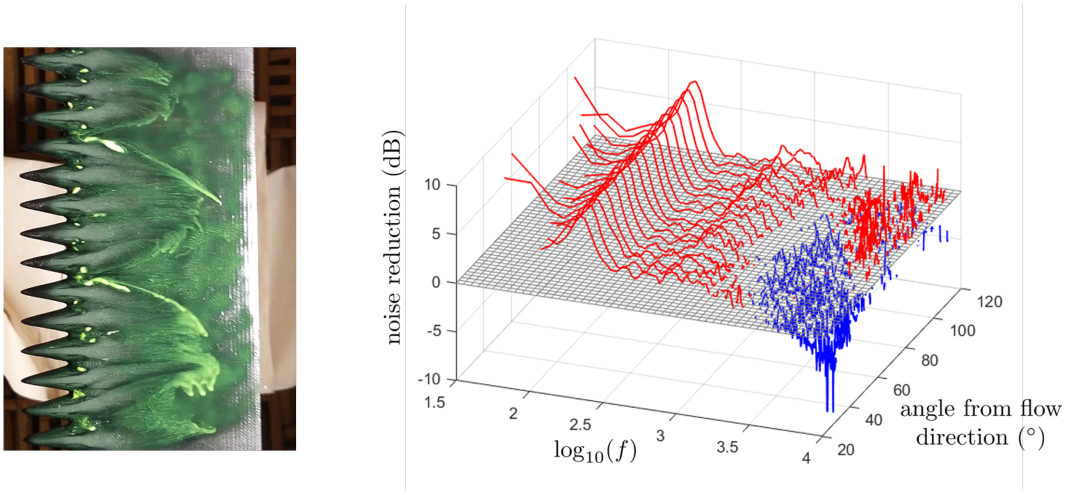

Figure 1.1: (a):visualisation of stall cells on a NACA-0012 airfoil at large angle of attack in clean flow, from ECL tests during the project *SmartAnswer*. (b): associated noise-reduction spectra.

3 Leading-Edge Serrations or Tubercles

Leading-edge serrations or tubercles are mostly inspired by the fore-flippers of humpback whales. Though initially identified as a way to better manage the aerodynamic performance of airfoils by delaying stall, they have also been shown to strongly reduce the noise from impinging turbulence on airfoils, as evidenced, again, in many experimental studies and theoretical or numerical works. However, application to large wind turbines seems to be reduced to the one reported by Fish [11].

Apart from their twofold nature, the effects of leading-edge modifications are not decoupled from what happens at the trailing edge, which makes their assessment more challenging. For effective reduction of the noise from impinging turbulence, the geometrical wavelength of the serrations/tubercles must be of the same order of magnitude as the integral length scale of the oncoming turbulence. Experiments reported by Chaitanya *et al* [8] evidence a best-tuned serration wavelength of about four integral length scales of the oncoming turbulence. The also conclude to a best-performing serration-edge angle of about 75°. Now the characteristic integral length scales in atmospheric turbulence are of the same order of magnitude as the hub height, thus much larger than the blade chords [9]. With such a ratio of characteristic dimensions, a wavy LE would rather act at high frequencies associated with smallest turbulent eddies, close to the Kolmogorov scale. Because airfoil unsteady response at high frequencies is also reduced by LE-thickness effect [17], the interest of the tubercles/serrations is partly lost. Furthermore, a large variability is expected in practice. This makes the benefit of this technology for turbulence-impingement noise reduction quite hazardous. But the second effect of delayed stall is beneficial. It is more essentially in the sense that the post-stall aerodynamic performances are increased. As a result, the associated stall noise is possibly reduced. This effect, evidenced in preliminary experiments performed within the scope of the project *SmartAnswer*, is attributed to the fragmentation of the stall cells, as shown in Fig. 1.1-a, with shorter separated areas and faster reattachment. Logically, different stall/reattachment features trigger different states of the flow near the trailing edge, resulting in different trailing-edge noise signatures. The total noise of the stalled airfoil was found reduced in the low-to-middle frequency range, and slightly increased in the very-high frequency range, at some radiation angles, by sinusoidal tubercles (Fig. 1.1-b).

4 About Small-Scale to Full-Scale Transposition

The main concern with wind-tunnel tests of airfoils is that they are performed at typical Reynolds numbers that are much lower than the Reynolds numbers of full-scale blade segments. This makes some details of the flows over tested mock-ups possibly questionable. The best approach for transposing the observed aeroacoustic features in the laboratory experiment to full scale remains an open question, of crucial importance, especially when dealing with the large horizontal-axis wind turbines. In the special case of the assessment of broadband-noise mitigation devices, such as the serrations or tubercles addressed in this report, the question is even more sensitive. A simplified dimensional analysis can be proposed as a first step in the discussion. Roughly speaking, the blades of very large wind turbines are designed with chord lengths nearly inversely proportional to the blade cross-section radius, at least on the outer part of the disc excluding the closest area to the nacelle. Typical aspect ratios are about $c_m/R_t \simeq 40$, if R_t denotes the tip radius and c_m the minimum chord at tip. Therefore, if the inner part is ignored as not representative of the broadband noise, the chord-based Reynolds number is nearly constant along the span, with the order of magnitude

$$Re_\Omega = \frac{\Omega c\, r}{\nu} = \frac{\Omega c_m\, R_t}{\nu} \simeq \frac{\Omega R_t^2}{40\,\nu}\,.$$

Written differently in terms of tangential speed V_t at blade tip, $Re_\Omega = V_t R_t/(40\,\nu)$, so that the Reynolds number appears as logically proportional to the size of the wind turbine, assuming a fixed value of the achievable velocity V_t, compatible with fixed values of angle of attack and wind speed. For a moderately large wind turbine, $c_m \simeq 1\,\mathrm{m}$, $R_t \simeq 40\,\mathrm{m}$ and the tangential speed of $80\,\mathrm{m/s}$ corresponding to a tangential tip Mach number of about 0.24, Re_Ω is beyond $5\,10^6$, well in the supercritical regime of airfoils. Blade design also involves a decreasing cross-section thickness with increasing radius. Turbulent boundary layers must be considered on the blades, except for possible, though not highly probable, laminar unstable flow regimes associated with laminar instabilities, on the one hand, and separation or dynamic-stall regimes, on the other hand. The latter is much more likely to occur, because of variable conditions due to wind gusts and operation through the atmospheric boundary layer. Up to that point, the atmospheric boundary-layer thickness δ is larger than the nacelle height H added to the tip radius R_t, so that the wind turbine is totally embedded in the mean shear of the boundary layer. Possibly strong variations of the angle of attack are encountered, especially by the outer part of the blades, during one revolution. Such variations are able to induce dynamic stall at the rotational frequency on each blade. Regimes of dynamic stall in airfoil experiments are characterized by the ratio $k = \pi\, f_0 c/U_0$, if f_0 is the frequency of the oscillations of angle of attack and U_0 the relative speed on the airfoil. With the aforementioned assumption of nearly constant chord-to-radius ratio and typical values, $f_0 \simeq 1/\pi$ and $k = c/(2r) \simeq 0.0125$ is also nearly constant along the span. This value is quite small, suggesting quasi-steady dynamic stall, if any. A reduced ratio k^* is also defined as $\alpha_1\, k$, α_1 denoting the half amplitude of the oscillations in angle of attack, in radians. α_1 is related to the parameters H and δ, more precisely the vertical wind-speed gradient experienced by the considered blade segment, noted $a = \mathrm{d}V/\mathrm{d}z$, if wind bursts are ignored. The instantaneous angle of attack can be evaluated as

$$\alpha = \gamma - \tan^{-1}\left(\frac{a\,(H - r\,\cos\Omega t)}{\Omega\, r}\right)\,,$$

from which typically α_1 is found about 4-5° for a gradient of $a = 5/40$. This leads to the estimate of $k^* \simeq 1.1\,10^{-3}$, confirming the quasi-steady regime.

The analysis suggests that the effect of serrations could be only performed in static conditions. However, the absence of dynamic-stall data with serrated airfoils motivates a dedicated experiment. As long as realistic values of the relative speed are reached, which requires the highest achievable performance of the wind tunnel in the present case, the Mach similarity is obtained. But typical mockups are 1/10-scaled, which means that tests are performed at 10 times too small Reynolds numbers, or even below, typically in the range 10^5-$5\,10^5$. This corresponds to the transitional regime or the high sub-critical regime, depending on the airfoil design. Implementing serrations prevents the need for artificial tripping devices to avoid laminar instabilities, because the serrations are known to deactivate the instabilities and/or their amplification by acoustic feedback. However, relative boundary-layer thicknesses over the airfoil surfaces are artificially thicker for lower Reynolds numbers, for the same assumed regime of developed turbulent boundary layers. It is known from the literature on trailing-edge serrations that the geometrical wavelength of the serrations λ_s must be tuned to the correlation length of the turbulence convected past the trailing edge. The latter can be assumed proportional to the airfoil boundary-layer thickness δ_c. This means that any λ_s/c ratio tested on a mockup should be rescaled as a smaller value for transposition at full scale. If classical results for laminar boundary layers are accepted (more convincing scaling laws for turbulent boundary layers should be used, but the very variable effect of the longitudinal pressure gradient makes the estimate very imprecise), Blasius' expression, cited by Schlichting [18] states that

$$\delta_c \sim 0.36\, x\, Re_x^{-1/5}\,,$$

if Re_x is the Reynolds number based on some length x, here assimilated to the chord length. This leads to the factor 0.6 to be applied on δ_c/c, thus on λ_s/c. The length of the serrations, in contrast, is tuned proportionally to λ_s in order to have a large serration-edge angle. This could still be questioned by the installation effects of open-jet wind tunnels, for which it is recognized that geometrical angles of attack and associated nozzle-flow deviations reduce the effective angle of attack, when also modifying the chordwise pressure gradient, thus the developing boundary layers. Furthermore, stall involves characteristic scales of the same order of magnitude as the chord length and the span. In either static or dynamic conditions, this can increase the blockage effect in wind tunnels of relatively narrow flows, and/or induce confinement effects, because of the mounting between end-plates.

Chapter 2

Experimental Setup and Airfoil Design

1 Tested Airfoil Mockups

Various versions of the baseline and modified NACA-63_3418 airfoil have been manufactured, taking the opportunity of the experiment to also assess 3D-printing and test the effect of the material in this manufacturing technology. In particular, the effect of allowing for some porosity of the material on airfoil self-noise remains an open question. The denomination and geometry of the versions are listed below, associated with mock-ups from left to right in Fig. 2.1.

- N1 baseline airfoil made of aluminum, with pressure-side tripping (the same as used for PIV measurements)
- N2 3D-printed baseline airfoil, plain material
- N3 3D-printed baseline airfoil, porous material
- N4 modified airfoil with wavy leading-edge; serration wavelength 20 mm
- N5 modified airfoil with wavy leading-edge; serration wavelength 10 mm
- N6 modified airfoil with trailing-edge serrations of wavelength 3 mm

All wavy-leading edge shapes are defined around the baseline straight edge line, so that all airfoils have the same area. In contrast, the serrations of the N6 version are add-ons inserted in a slit after trailing-edge truncation, without final step along the airfoil surface, not significantly extending the baseline chord length. Because the aerodynamic loads concentrate in the leading-edge area, this choice makes less deviations expected from constant aerodynamic performances, thus more reliable acoustic comparisons. However, slightly degraded aerodynamic performances, say lift decrease and drag increase, are a commonly reported fact. The leading-edge and trailing-edge devices have been tested independently. Combined leading-edge tubercles and trailing-edge serrations could be of interest for a future work.

2 Microphone Locations and Investigated Flow Regimes

14 far-field microphones positioned along a horizontal arc are used, as shown in Fig. 2.2. The angles are defined from the downstream direction of the wind-tunnel incident flow.

- Left-bank microphones M1 90°, M2 80°, M3 70°, M4 60°, M5 50°, M6 40° and M7 100°

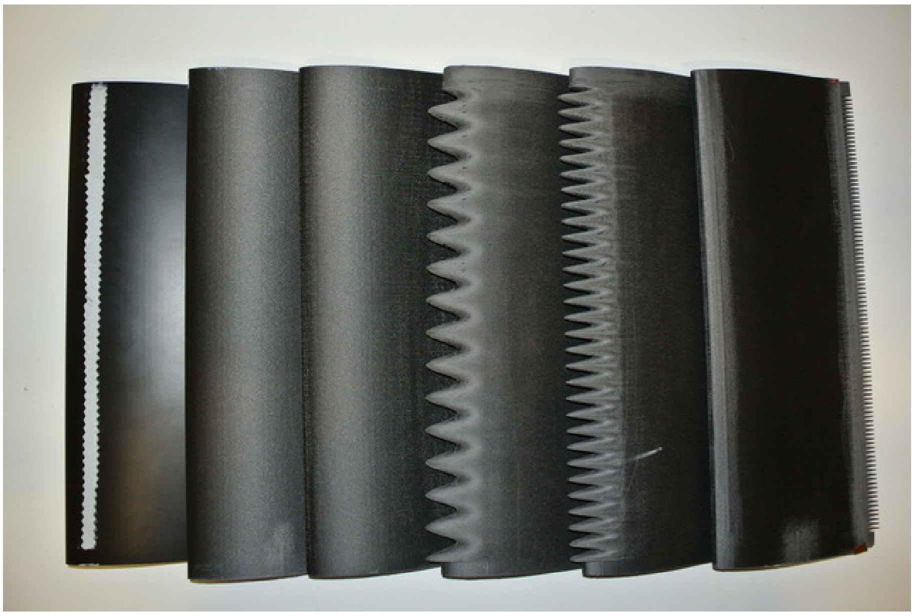

Figure 2.1: Picture of the baseline and modified versions of the NACA-0012, N1 to N6 used in the experiment.

- Right-bank microphones M8 100°, M9 40°, M10 50°, M11 60°, M12 70°, M13 80° and M14 90°

All tests have been performed in clean flow conditions, with the negligible residual turbulent intensity of the wind tunnel. The investigated flow regimes in static conditions are:

- U=25 m/s or 50 m/s
- geometrical angle of attack 6°, 10°, 15°, 18°, 22° and 27°
- acquisition time of signals 30 s

The flow regimes investigated in dynamic-stall conditions are:

- oscillation amplitude 15° around 15°
- U=25 m/s: 3 oscillation frequencies 0.663 Hz, 1.658 Hz and 3.316 Hz corresponding to the reduced frequencies $k = 0.01$, $k = 0.025$ and $k = 0.05$ (associated acquisition times 151 s, 61 s and 31 s).
- U=50 m/s: 3 oscillation frequencies 0.663 Hz, 1.326 Hz and 3.316 Hz corresponding to the reduced frequencies $k = 0.005$, $k = 0.01$ and $k = 0.025$ (associated acquisition times 151 s, 76 s and 31 s).

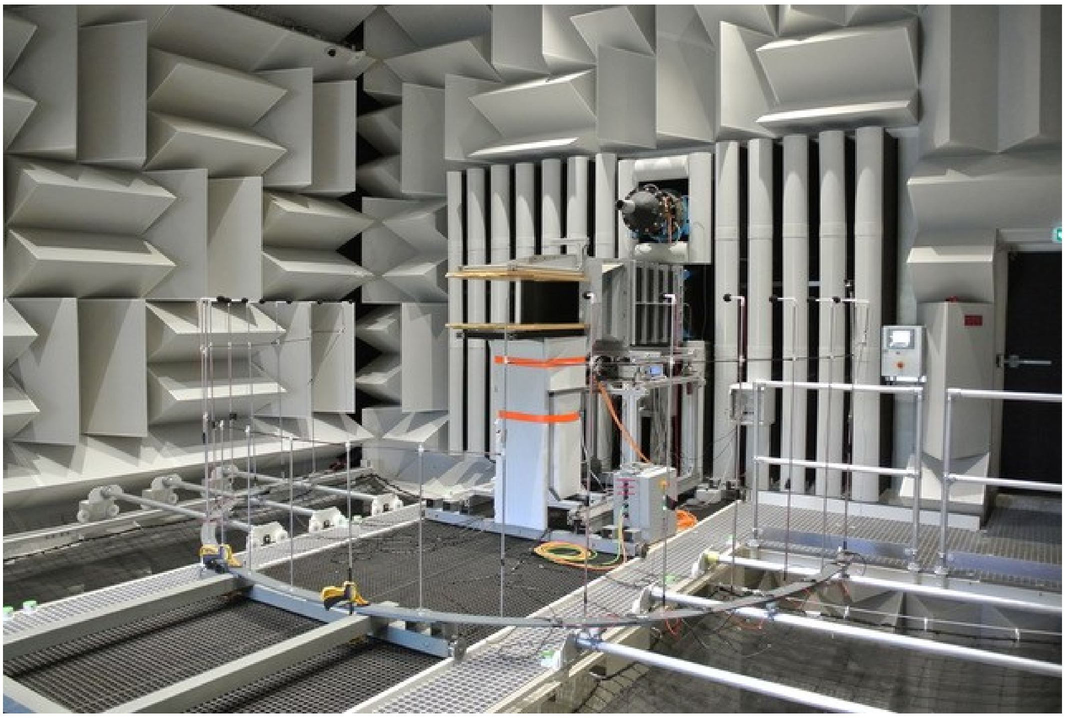

Figure 2.2: Downstream-oblique view of the experimental setup in the large anechoic open-jet facility of ECL.

Chapter 3

Measurements in Static Conditions

This part is dealing with the tests performed at various angles of attack including stall regime, in static conditions. Far-field sound spectra measured at some angles are compared. The emphasis is on the results for a flow speed of $U = 50\,\mathrm{m/s}$, more representative of the high Reynolds numbers expected in applications.

1 Background-Noise Correction

Far-field sound spectra of the N1-airfoil, measured at angles $\pm 90°$ (microphones M1 and M14) with respect to the direction of the incident flow, are plotted in Fig. 3.1, for the tested geometrical angles of attack. All spectra are representations of Power Spectral Densities (PSD) in dB/Hz (the acquisition frequency is 51.2 kHz and averaging is performed on a 8-Hz bandwidth) Raw spectra are shown in Fig. 3.1-a and -b, where the background noise spectra are in gray, and corrected spectra after background-noise subtraction are displayed in Fig. 3.1-c and -d. At zero angle of attack, the N1-airfoil radiates low noise, in the middle-and-high frequency range, whereas much more substantial noise is radiated at high angles of attack, with significant increase, also in the low-frequency range. The angle 27° exhibits the characteristic low-frequency peak of the stall regime, around 160 Hz. In contrast, intermediate angles correspond to a dominant broadband signature ranging from 300 Hz to 1.5 kHz. Furthermore, in the high-frequency range beyond 2 kHz, the noise increases regularly with the angle of attack.

2 Effect of Manufacturing Process

Sound spectra measured at the microphone M14 for the three versions of the baseline NACA-0012 airfoil are compared in Fig. 3.2, to assess the effect of the material and the manufacturing process.

Because the N1 version in aluminum is tripped in the front part, the tripping device is likely to trigger a different boundary-layer development. In particular, transition to turbulence is accelerated. Typically, the high-frequency tonal noise of the non-tripped, 3D-printed version N2, seen at angles of attack of 0° and 10°, is not observed with the other two. The tones are attributed to laminar instabilities, often referred to as Tollmien-Schlichting (TS) waves, amplified by acoustic feedback. This means that the surface of the N2 airfoil is smooth enough to keep laminar boundary layers under low loading conditions, and that, by the way, no artificial effect of increased roughness is induced. The porosity of the version N3 seems to deactivate the TS-wave radiation, either because of increased equivalent roughness or permeability.

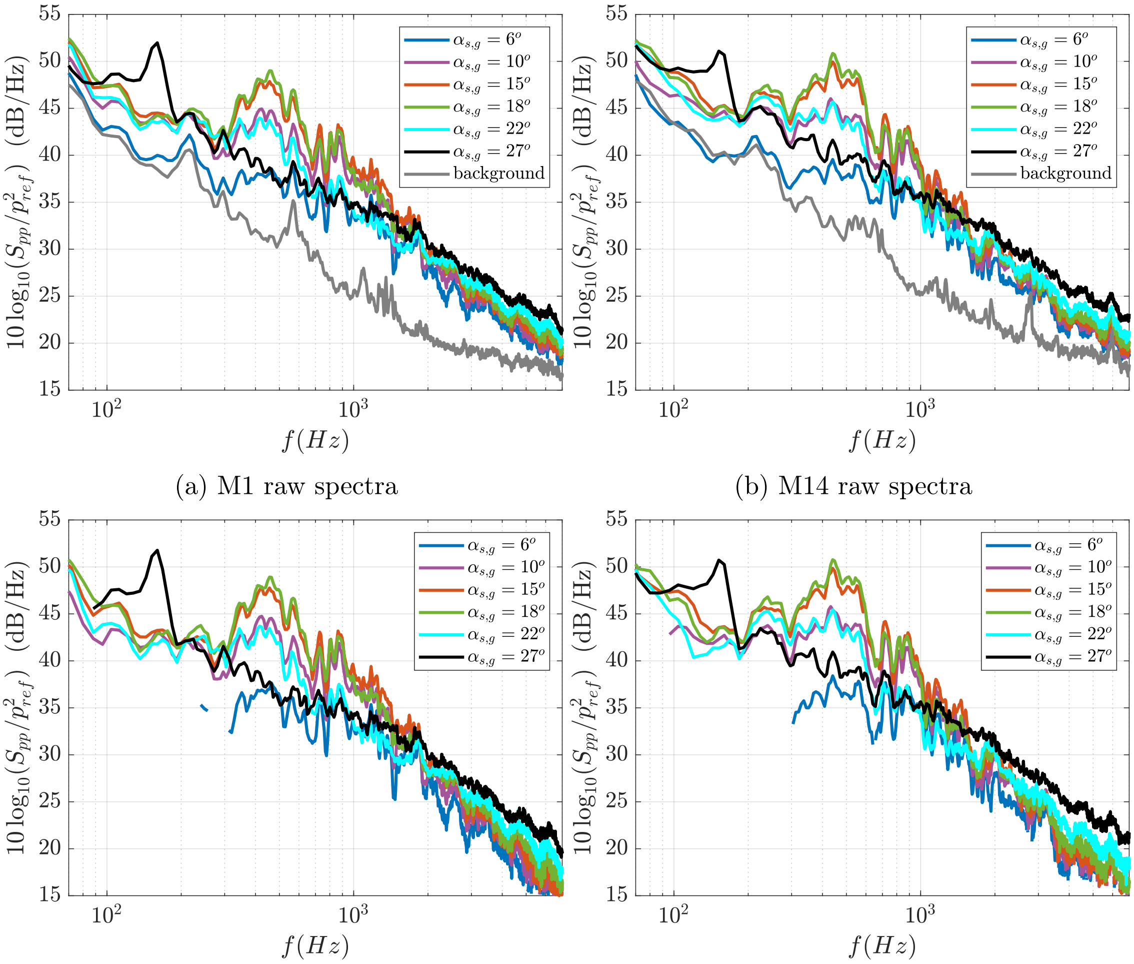

(a) M1 raw spectra

(b) M14 raw spectra

(c) M1 after background-noise subtraction

(d) M14 after background-noise subtraction

Figure 3.1: Compared spectra for the N1 airfoil (aluminum) at various angles of attack, with and without background-noise (BGN) subtraction. Microphones at ±90°.

3 Effect of a Wavy Leading Edge

Again, the microphone M14 is selected in this section. The airfoil N2 is taken as baseline and compared to versions N4 and N5, corresponding to longer and shorter wavelengths of the wavy cut, respectively. This choice ensures that the comparison is reliable, as made for mockups manufactured with the same process. The tonal trailing-edge noise of the N2 airfoil at low angles of attack, attributed to laminar instabilities, must be discarded from the analysis, as not representative of the expected broadband noise on a full-scale wind turbine. Apart at the angle of attack 18°, clear global trends are evidenced. The larger serrations of the N4 airfoil lead to a quite large noise increase, especially at the large angles of attack representative of deep stall. The opposite is observed with the smaller serrations of the N5 airfoil, leading to a substantial noise reduction at the same angles. The measured noise levels with small serrations are almost systematically lower than those measured with the large serrations. Further investigation is needed to elucidate why the different scales and dimension ratios lead to so different acoustic signatures, with the same technology. A different structure of the stall cells, illustrated for the NACA-0012 airfoil in Fig. 1.1, is a possible explanation, still to be confirmed in the present case. The strong noise increase observed with the two serrated airfoils at low frequencies and at the angle of attack 18°, is unexplained. Its origin should be related to the formation of large-scale fluctuating flow patterns.

4 Effect of Trailing-Edge Serrations

The effect of triangular serrations is reported in this section by comparing the baseline airfoil N2 and the serrated airfoil N6, for the microphone M14. Sound spectra are plotted in Fig. 3.4. At the smallest angles of attack, the tonal noise radiated by the baseline airfoil and attributed to laminar instabilities is suppressed, because the serrations deactivate the acoustic feedback, essentially by introducing spanwise de-correlation. Though laminar instabilities are not likely to develop on full-scale wind-turbine blades, because of the much higher associated Reynolds numbers, this effect of serrations must be noted. It has been already observed in previous works. A significant reduction of the middle-to-high frequency broadband noise is also achieved by the serrations at low and moderate angles of attack. Noise is increased in a range of low frequencies, typically a couple of hundred Hz, at all angles of attack. This trend is quite unexpected. Indeed, trailing-edge serrations are more identified as a device which regenerates sound at very high frequencies, because of the cross-flow induced around the serrations, from the pressure to the suction side.

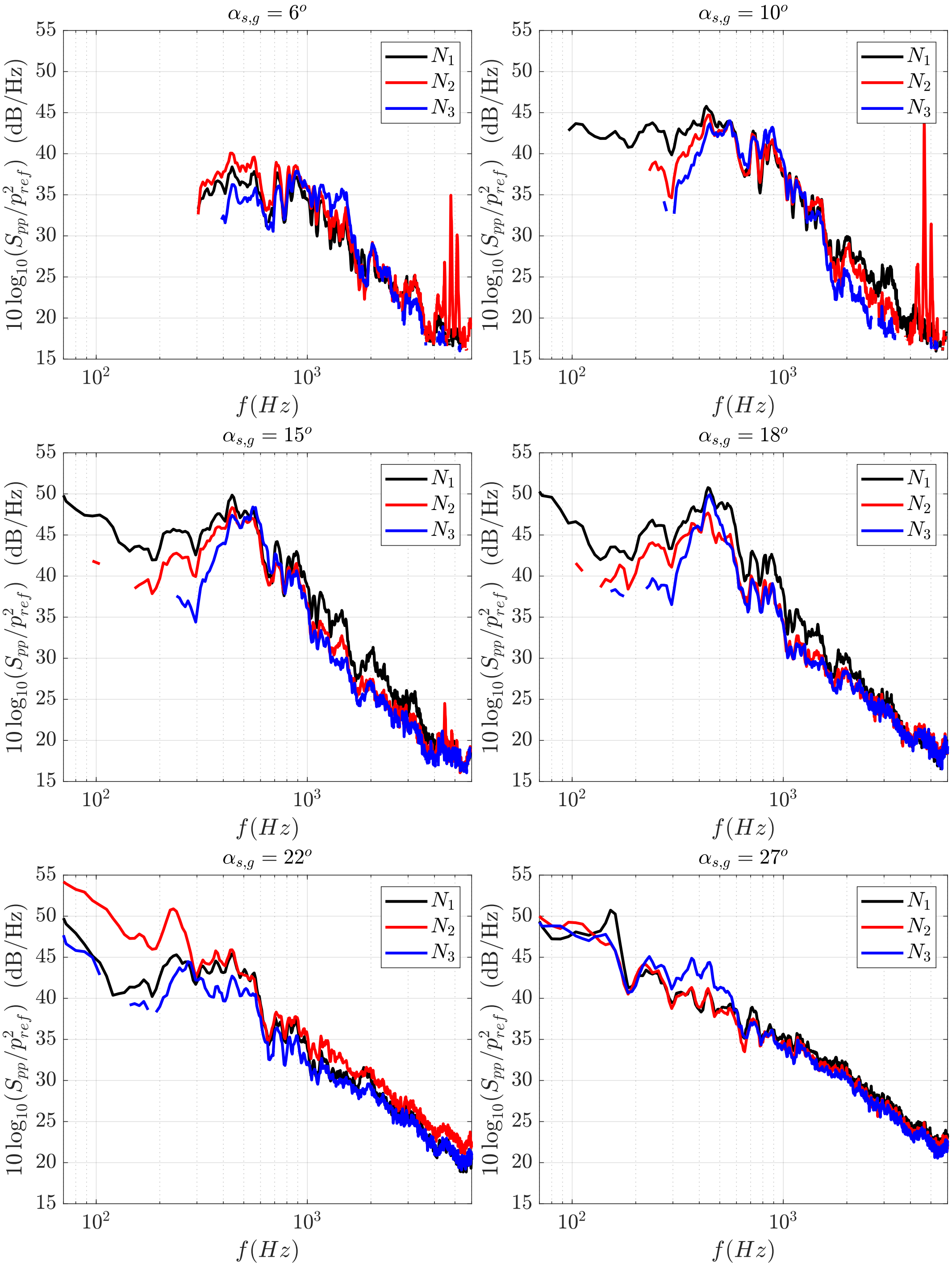

Figure 3.2: Compared sound spectra of the airfoils N1 (aluminum), N2 (plain 3D-printed) and N3 (porous 3D-printed). Background noise subtracted. Microphone M14.

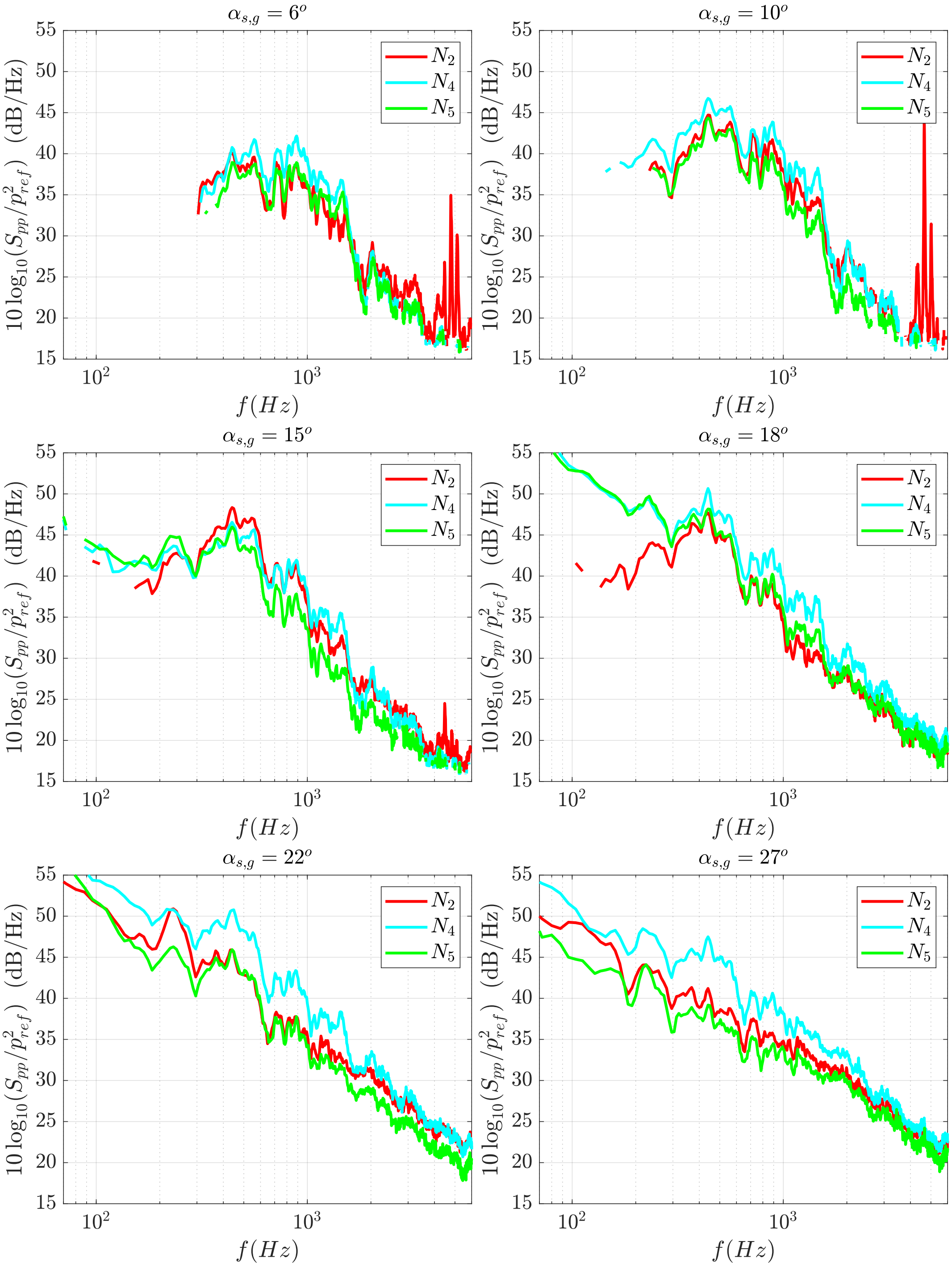

Figure 3.3: Compared sound spectra of the airfoils N2 (straight edge), N4 (wavy cut $\lambda = 20\,\text{mm}$) and N5 (wavy cut $\lambda = 10\,\text{mm}$). Background-noise corrected, microphone M14.

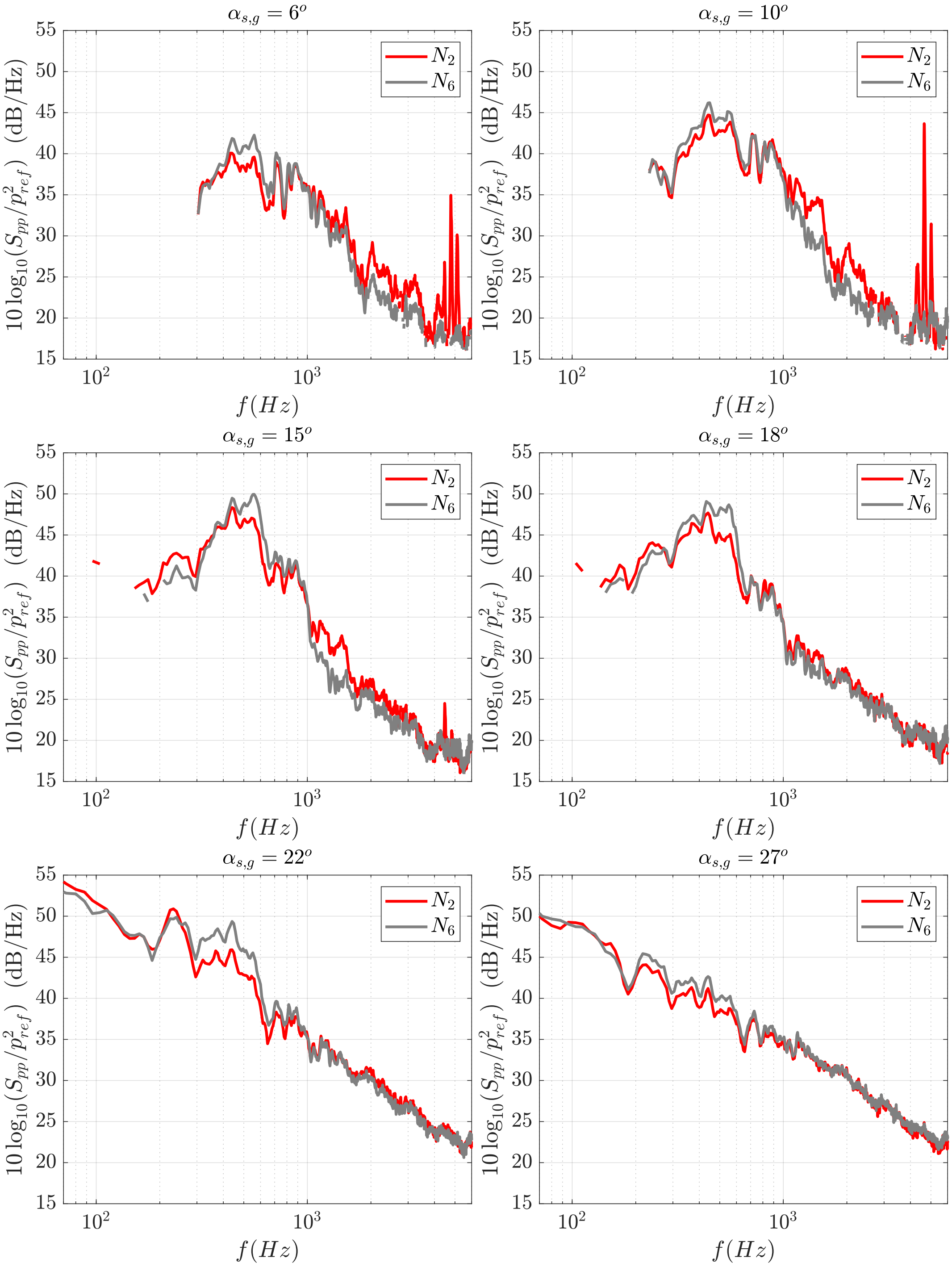

Figure 3.4: Compared sound spectra of the airfoils N2 (baseline) and N6 (trailing-edge serrations $\lambda = 3\,\mathrm{mm}$). Background-noise corrected, microphone M14.

Chapter 4

Measurements in Dynamic-Stall Conditions

The results presented in this chapter are for an incident flow speed of $U = 50\,\mathrm{m/s}$, the amplitude $15°$ of the oscillations of angle of attack around the averaged geometrical angle of attack $15°$, at a frequency $1.30\,\mathrm{Hz}$ corresponding to the reduced frequency $k = 0.01$.

1 Selection of Parameters For the Spectral Analysis

The analysis is based on a time-frequency analysis of the measured signals. Two sets of parameters are tested for the calculation of standard spectrograms of the conditioned, phase-averaged acoustic pressure, as detailed in Table 4.1.

1. In the first set, each cycle of duration $t_c = 769\,\mathrm{ms}$ is split into 10 periods of 3937 samples. With an overlap of 80%, this leads to a time step $\Delta t = 15.4\,\mathrm{ms}$. Spectra are computed with $N = 2^{13} = 8192$ points, which corresponds to a frequency resolution $\Delta f = 6.25\,\mathrm{Hz}$ at the present sampling frequency of $F_e = 51.2\,\mathrm{kHz}$.

2. In the second set, each cycle of duration $t_c = 769\,\mathrm{ms}$ is now split into 20 periods of 1969 samples. The same overlap of 80% leads to a time step $\Delta t = 7.7\,\mathrm{ms}$. Spectra are computed with $N = 2^{12} = 4096$ points, which corresponds to a frequency resolution $\Delta f = 12.5\,\mathrm{Hz}$ at the same sampling frequency.

The phase-averaged spectrograms in figure 4.1 exhibit a peak (horizontal bar) around 220 Hz, the width of which is larger with the set 2 of parameters, because the frequency resolution is poorer. In counterpart, the transients are better captured with the set 2. This effect is more clearly evidenced in figure 4.2, plotting the overall sound pressure level in decibels, calculated by integration on the spectrograms between 75 Hz and 25 kHz, or between 75 Hz and 1 kHz. For the baseline airfoil N1, the peaks observed at the times of separation and reattachment are substantially narrower with the time resolution of 7.7 ms. In contrast, no clear difference is seen in the case of the airfoil N2, for which transitions appear smoother.

Table 4.1: Parameters for the calculation of phase-averaged spectrograms.

Set of parameters	1	2
Δt (ms)	15.4	7.7
Δf (Hz)	6.25	12.5

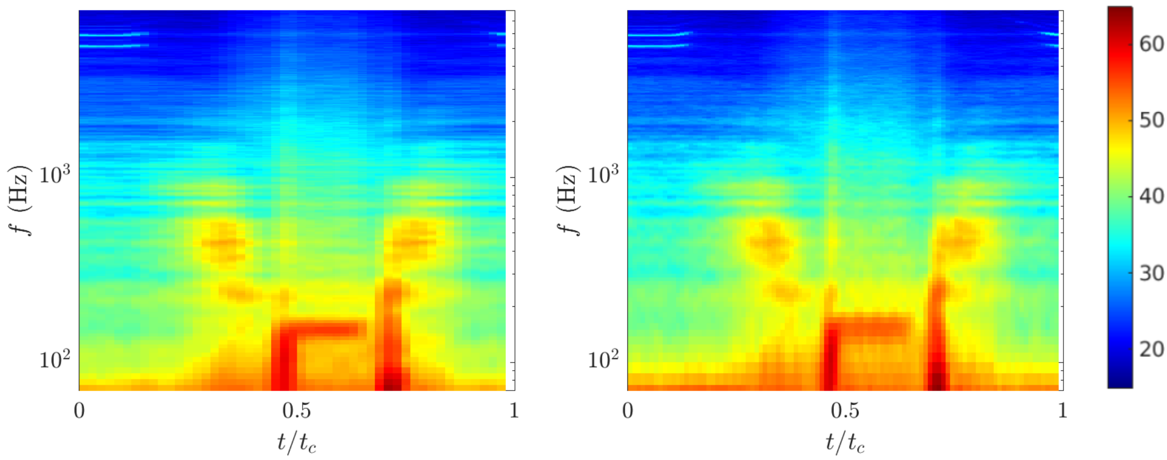

(a) airfoil N1 - $\Delta t = 15,4\,\mathrm{ms}$ (b) airfoil N1 - $\Delta t = 7.7\,\mathrm{ms}$

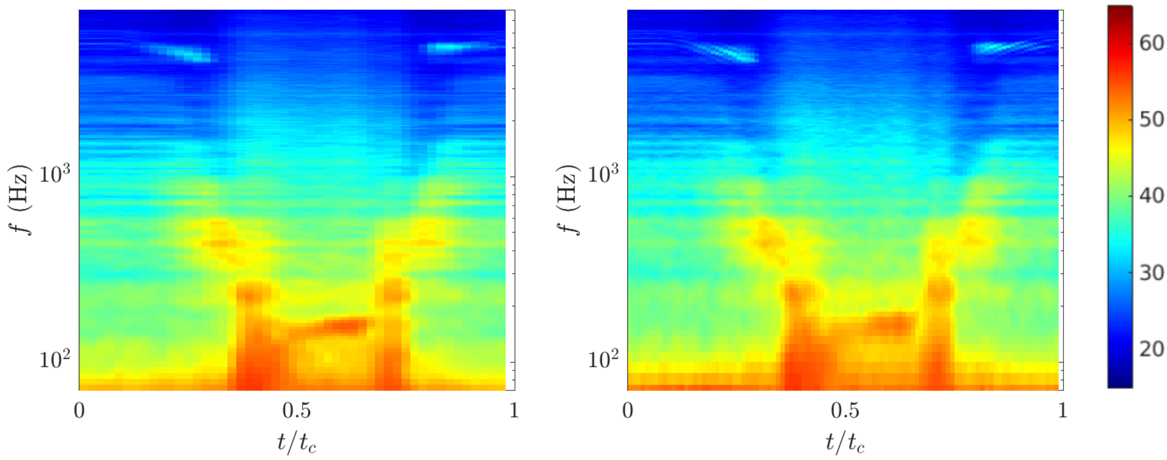

(c) airfoil N2 - $\Delta t = 15,4\,\mathrm{ms}$ (d) airfoil N2 - $\Delta t = 7.7\,\mathrm{ms}$

Figure 4.1: Phase-averaged spectrograms of the microphone M14, for the baseline airfoils N1 (aluminum) and N2 (3D-printed), and for the two sets of parameters.

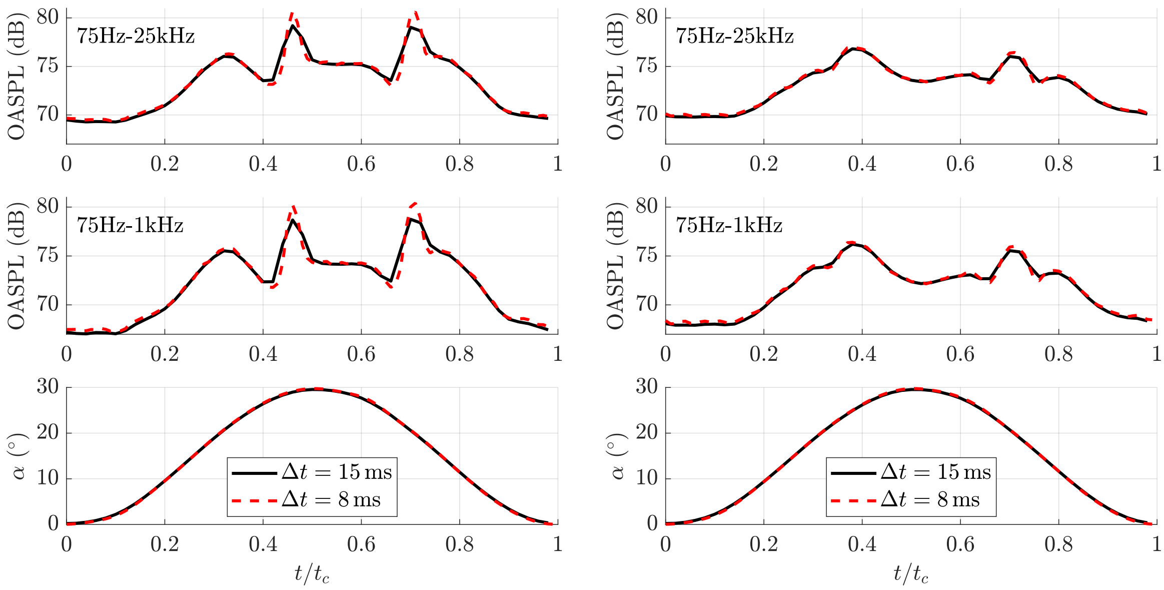

(a) airfoil N1 (b) airfoil N2

Figure 4.2: Phase-averaged filtered OASPL between 75 Hz and 25 kHz (top) or between 75 Hz and 1 kHz (middle) for the microphone M14. Airfoils N1 (aluminum) and N2 (3D-printed), two sets of parameters. Variations of angle of attack on the bottom plots.

2 Comparison of Time-Frequency Signatures

Phase-averaged spectrograms of the signals at the microphone M14, calculated for the airfoils N2 (baseline), N4 and N5 (wavy leading edges), and N6 (serrated), are compared in figure 4.3. The set 1 of parameters is used.

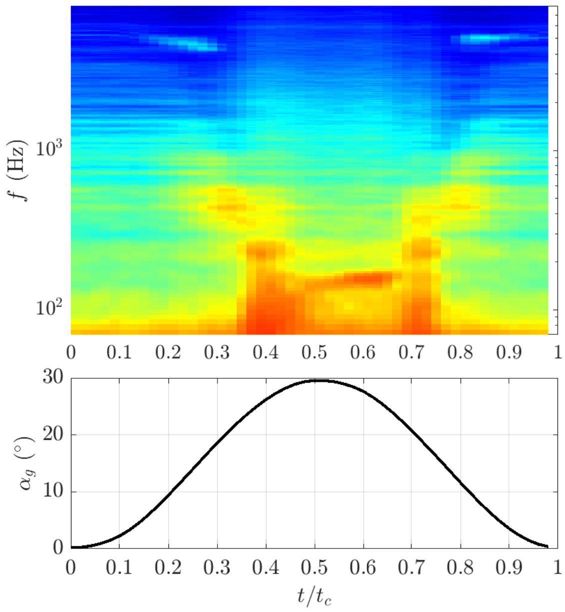

(a) airfoil N2 (baseline)

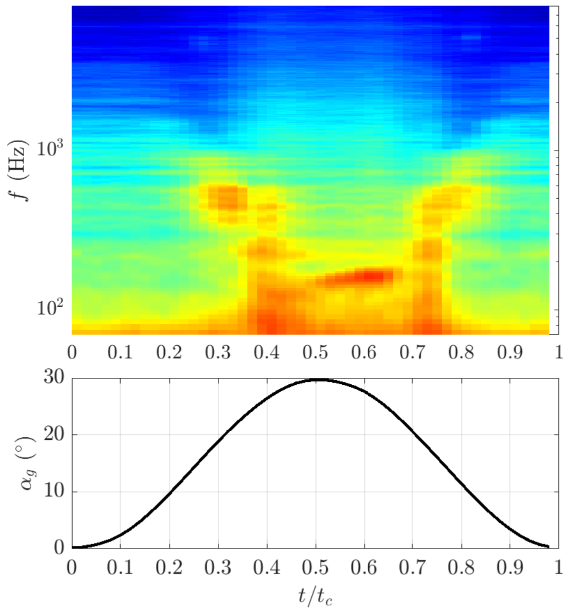

(b) airfoil N6 (serrations $\lambda = 3\,mm$)

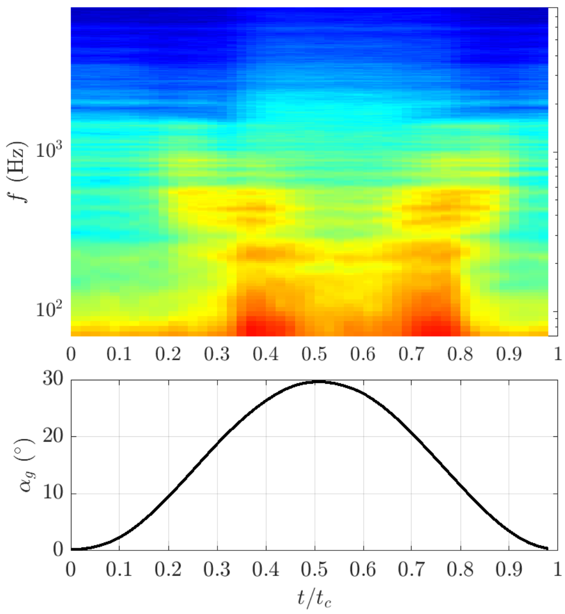

(c) airfoil N4 (tubercles $\lambda = 20\,mm$)

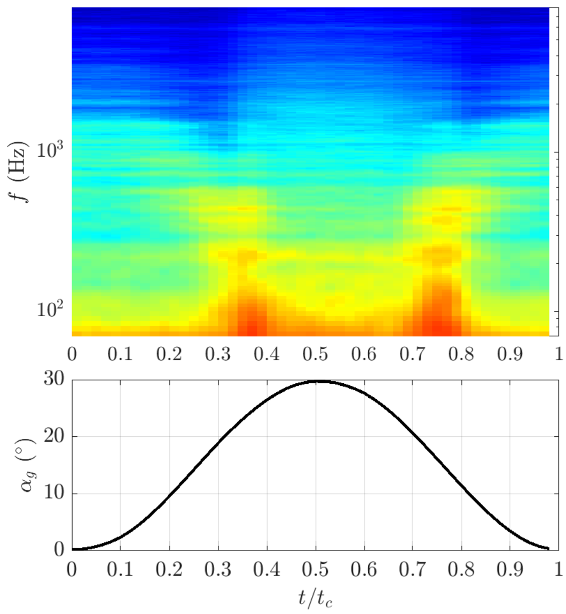

(d) airfoil N5 (tubercles $\lambda = 10\,mm$)

Figure 4.3: Phase-averaged spectrograms for microphone M14 and various airfoil versions. $\Delta f = 6.25\,\mathrm{Hz}$. Color scale from 15 to 65 dB. Time-variations of angle of attack indicated below each color map.

Trailing-edge serrations alone seem to globally increase the radiated noise, while keeping the general pattern of the spectrogram unchanged. In particular, the red, slightly oblique bar between the signatures of separation and reattachment, is maintained Leading-edge tubercles of both versions N4 and N5 are found to make the pattern more symmetrical, with less concentrated events in time. Furthermore, the narrow-band peak (red bar in the spectrograms) found with the other two airfoil versions, N2 and N6, and associated with the large-scale vortex shedding or buffeting characteristic of deep stall, is effectively reduced, as clearly seen later in Figure 4.5-c. The red bar is suppressed at the benefit of a horizontal trace of lower amplitude at higher frequency. Furthermore, a clear overall reduction of the noise pattern is found with the smaller-wavelength tubercles of the airfoil N5, making this design a promising candidate for noise mitigation in applications. In particular, a lower-noise region is formed between the comparatively louder events at separation and at reattachment.

A possible reason for the best performance of the airfoil N5 is the formation of fragmented separated areas, as shown in Fig. 1.1, associated with faster reattachment before the trailing edge. A more massive separation is observed in small-scale wind-tunnel experiments with straight-edged airfoils. This is supposed to reduce the coherence of large-scale, low-frequency motion in the flow. As discussed in section 4, the present observations are made for typical Reynolds numbers about ten times smaller than those of full-size large wind turbines. This could question the validity of transposition. But because the tubercles also force to reconsider the criteria of natural transition to turbulence on an airfoil by largely increased three-dimensional effects, the low-Reynolds number effects could be less critical than for straight-edged airfoils. The main concern about leading-edge tubercles rather arises from the manufacturing issues at the scale of a large wind turbine.

3 Time Variations of Filtered OASPL and Directivity Considerations

Time-variation profiles of the filtered OASPL between 75 Hz and 1000 Hz are plotted in Fig. 4.4, for a more quantitative assessment of the differences between airfoil versions pointed on the aforementioned spectrograms. This is done for both microphones M1 and M14. The times indicated by vertical dashed lines are used to extract instantaneous spectra, discussed in the next section.

A first typical result is the local maximum of OASPL emerging at intermediate time between the humps associated with separation and reattachment, for the serrated airfoil N6 (green plot). Also clear is the broader humps found with the airfoil N4, which goes with a louder signature. The global sound reduction achieved with the airfoil N5 is also clearly confirmed.

4 Analysis of Instantaneous Sound Spectra

For a complementary discussion, sound spectra extracted from the spectrograms, at the four times of the cycle indicated by dashed lines in Fig. 3.1b, are displayed in Fig. 4.5. Spectra for the four selected airfoil versions are superimposed. The extraction times correspond, successively, to the attached-flow phase, the first peak of separation, the deep-stall phase and the second peak at reattachment. Examination of the spectra confirms and completes aforementioned findings. The low-frequency peak characteristic of the deep-stall signature, around 160 Hz (Fig. 4.5-c), is suppressed by the leading-edge tubercles. But beyond the peak frequency, deep-stall broadband noise is increased with the N4 design, whereas it is decreased with the N5 design, both being the loudest and the quietest, respectively. Again, the versions N4 and N5 are the loudest and quietest at the first peak associated with separation. This could be explained by the expected 'delayed stall' with tubercles reported in the literature. In the attached-flow phase (Fig. 4.5-a), the leading-edge tubercles seem to cause some increase of noise in the middle-frequency range. Though confirmation is needed, this can be attributed to the additional vortex dynamics injected in the boundary layers, resulting in increased trailing-edge noise. The trailing-edge serrations of the airfoil N6 only provide a modest noise reduction at the highest frequencies, beyond, say 3 kHz. Trailing-edge serrations are found to produce negligible changes in the separation and deep-stall phases. A common drawback of the leading-edge tubercles is that they induce an increase of low-frequency broadband noise, of about 5-6 dB,

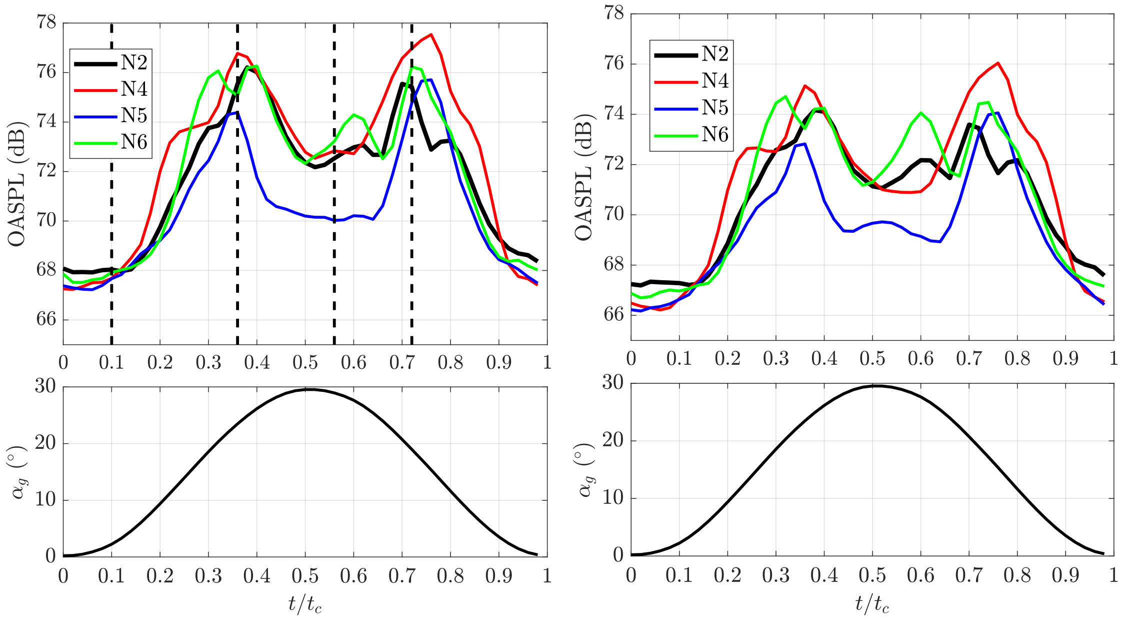

(a) Micro M14

(b) Micro M1

Figure 4.4: Cyclic time variations of the filtered OASPL from 75 Hz to 1000 Hz, for microphones M14 and M1. Vertical dashed lines point the times $t_1/t_c = 0.1$, $t_1/t_c = 0.36$, $t_1/t_c = 0.56$ and $t_1/t_c = 0.72$.

in the reattachment phase (Fig. 4.5-d). This feature is unexplained. The airfoil N4 is even more detrimental, since it is also associated with a similar increase in the middle-and-high frequency range. The bad performance of the version N5 at the time $t/t_c = 0.72$ must not be interpreted as a serious drawback. Indeed, it is balanced by the benefit at other times, as suggested by inspection of preceding figures.

5 Directivity Assessment of the Filtered OASPL

Discussions in the preceding sections deal with the fixed observation angles ±90° with respect to the direction of the incident flow (wind-tunnel axis). Now it must be noted that in the considered frequency range, the airfoil chord is almost compact. Therefore, the sources of the sound can be assimilated to an equivalent dipole, roughly perpendicular to the chord-wise direction. For a 15° angle of attack, the actual angles of the microphones are shifted by the same amount from ±15°, with respect to the chordwise direction. Moreover, during the dynamic-stall cycle, the additional variations make this inclined dipole still oscillate, not only in amplitude but also in orientation. Another effect to be considered is the refraction of sound waves emitted by the airfoil through the shear layers of the jet. The known result is an artificial tilting of the directivity lobes, as measured by far-field microphones located outside the flow, away from the downstream direction. In similar tests with a flat-plate airfoil at zero degree angle of attack, deviations of about 5° were found at a flow speed of 30 m/s [7]. A preliminary inspection of the directivity of the radiated sound, considered here for the previously defined filtered OASPL and without any correction, is plotted as a function of time in the dynamic-stall cycle and of observation angle in Fig. 4.6, in the form of a color map. The limited number of angles causes interpolation artifacts. Yet the results are clear enough for interpretation.

For a more quantitative assessment, directivity diagrams are also plotted for the four characteristic times of the dynamic-stall cycle, in Fig. 4.7. Corrections have not been considered here for two reasons. Firstly, their application is delicate in dynamic stall regime, because of the oscillatory motion of the jet. Secondly, existing models should be adapted for the curved sheared layers of a deviated jet, in cases of lifting airfoils. The fact

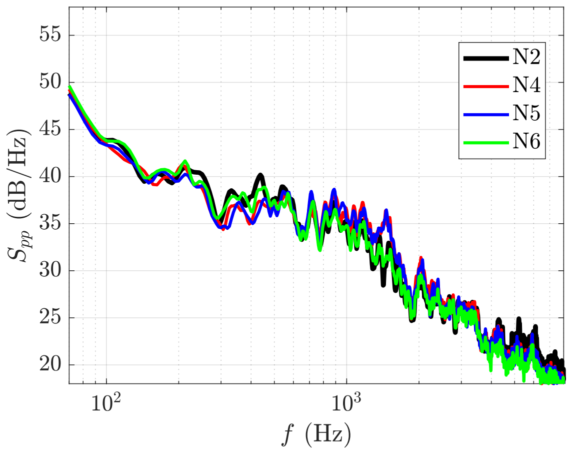

(a) $t/t_c = 0.10$ (attached)

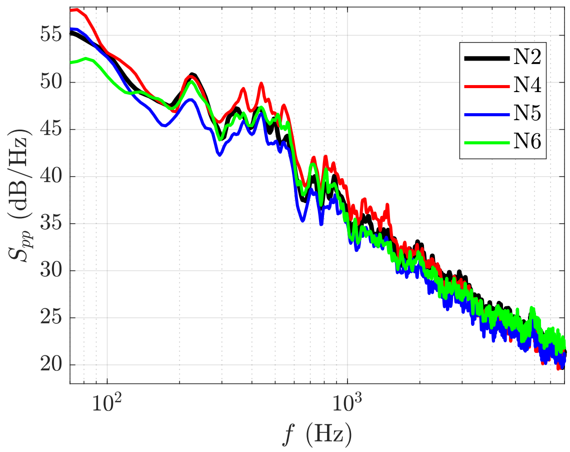

(b) $t/t_c = 0.36$ (first peak)

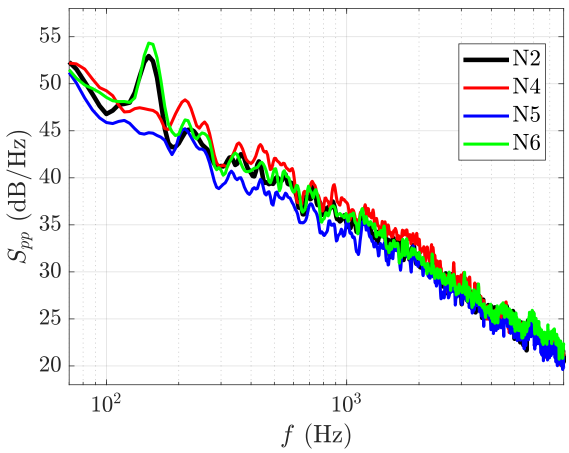

(c) $t/t_c = 0.56$ (deep stall)

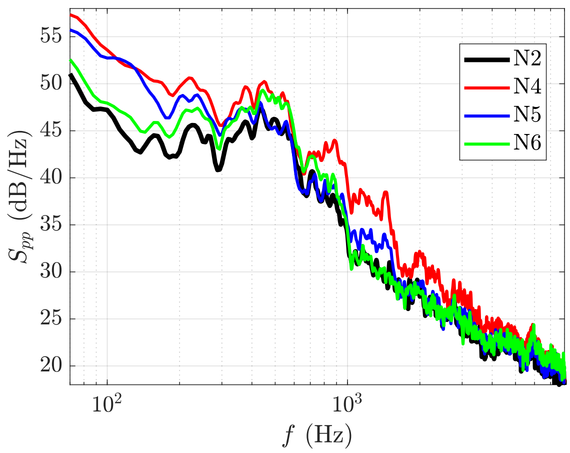

(d) $t/t_c = 0.72$ (second peak)

Figure 4.5: Phase-averaged sound spectra at microphone M14 for various airfoils at the four time steps t/t_c in figure 4.4. $\Delta f = 6.25\,\text{Hz}$.

that noise reductions are found the same at all angles in the present experiment makes such corrections optional *a posteriori*.

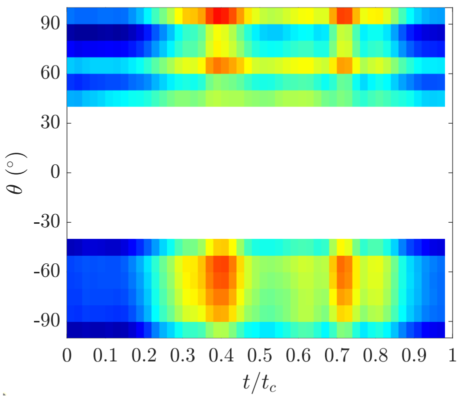

(a) airfoil N2 (baseline)

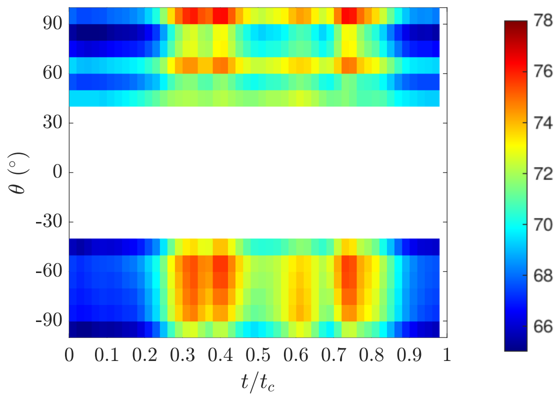

(b) airfoil N6 (serrations $\lambda = 3\,mm$)

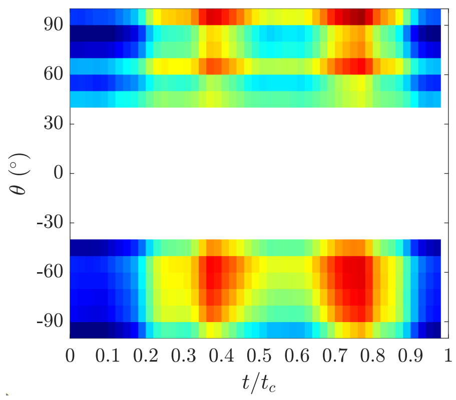

(c) airfoil N4 (tubercles $\lambda = 20\,mm$)

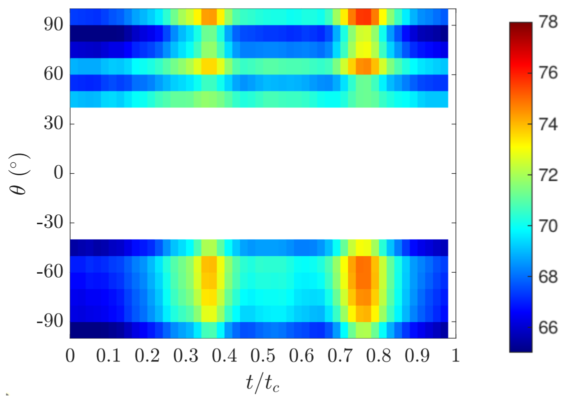

(d) airfoil N5 (tubercles $\lambda = 10\,mm$)

Figure 4.6: Directivity of the filtered OASPL between 75 Hz and 1000 Hz for the selected four airfoil versions.

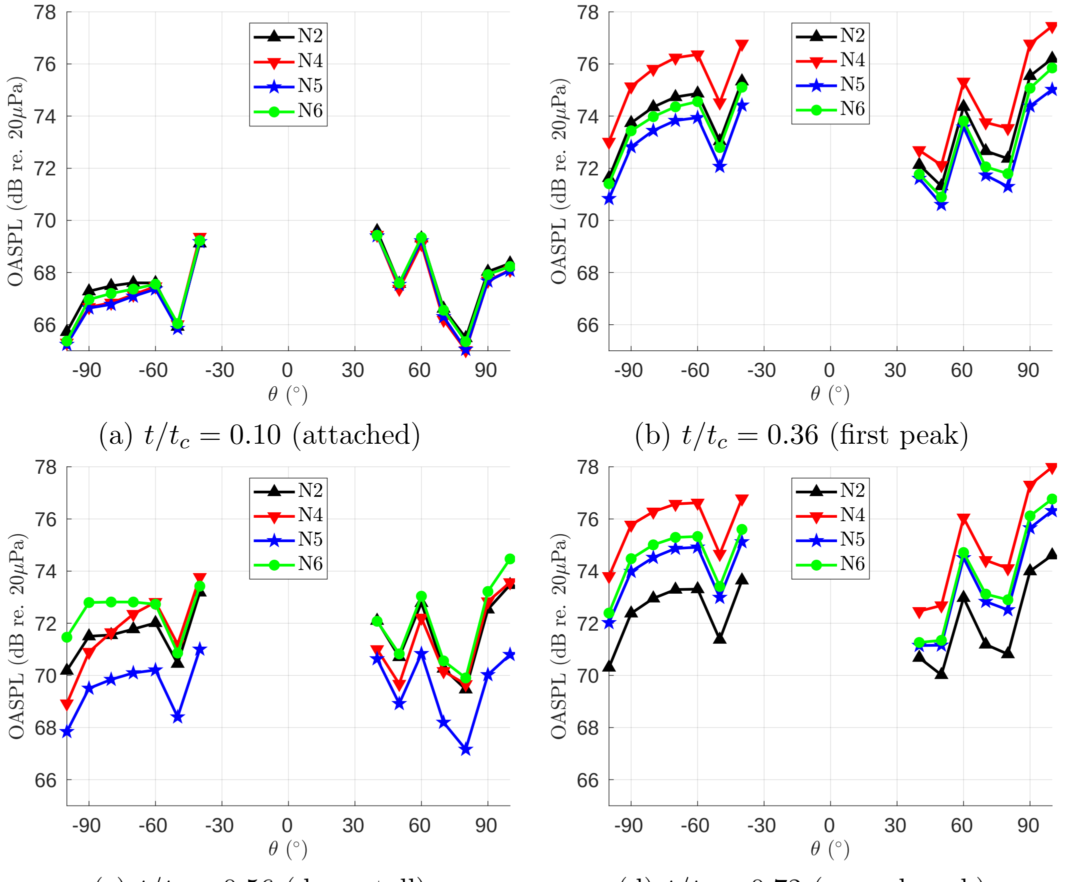

(a) $t/t_c = 0.10$ (attached)

(b) $t/t_c = 0.36$ (first peak)

(c) $t/t_c = 0.56$ (deep stall)

(d) $t/t_c = 0.72$ (second peak)

Figure 4.7: Directivity of the filtered OASPL between 75 Hz and 1000 Hz for the four airfoils at selected time steps t/t_c (see figure 4.4).$\Delta f = 6.25$ Hz.

Concluding Remarks

Several versions of the airfoil 63(3)-418, representative of wind-turbine blade design, equipped with noise-reduction devices, have been tested in an open-jet anechoic facility, both in static conditions at various angles of attack and in a regime of dynamic stall. The devices are either small-size trailing-edge (TE) serrations, or leading-edge (LE) serrations. In the latter case, the 3D-printing technology resulted in a smooth surface, free of irregularities or angular cuts, that would be responsible for artificial flow separation. Two LE serration designs, with relatively small and large serrations, have been considered.

Ignoring additional effects on the tonal trailing-edge noise associated with laminar instabilities, that would hardly be observed at full scale, the focus has been put on the broadband noise. Considering the global effects over a dynamic stall cycle, the small LE serrations have been found to effectively reduce the noise, whereas the large ones cause a dramatic noise increase. This suggests that best-tuned dimension ratios between the serration depth and wavelength, on the one hand, and presumably the airfoil chord and LE thickness, on the other hand, should be determined. TE serrations were found effective in high-frequency noise reduction, but in the same time detrimental for the noise at lower frequencies. Finally, the overall sound-level variations between tested configurations, in particular the reduction achieved with the most effective device, are independent of the angle of observation. They are reliable for three-dimensional extensions.

The present report focused on the results at the reference flow speed of 50 m/s. Data at other tested speeds would not question the main observation. They could be processed in a continuation of the study. It is also worth noting that leading-edge and trailing-edge devices have been tested separately and not combined, in order to clearly separate the benefits of each. Because separated and re-attached flows trigger variable conditions for trailing-edge noise, airfoils modified at both edges are *a priori* promising. Again, this could be the matter for future work.

Specific acoustic signatures observed in some configurations, for instance at 18° for the airfoils with serrated leading edges, are hard to explain with the limited knowledge of flow details. The present investigation was rather reduced to a minimum aeroacoustic characterization, so that a large number of configurations can be explored and promising designs identified. A deeper inspection of the unsteady flow features involved in dynamic stall in the presence of noise-mitigation devices would be of fundamental interest. Such an effort was beyond the scope of the present work.

About the transposition of results to full scale, the main concern is the artificially low Reynolds number. Many previous reported studies in research wind tunnels raised that point. One effect is that laminar unstable boundary layers can develop, instead of turbulent ones, leading to the emission of tones. This is usually avoided by adding tripping devices. No tripping is needed in the case of serrated airfoils, because the latter deactivate the acoustic feedback loops involved in the tonal self-noise. Another effect, more crucial, is that assuming the same flow regime, the boundary layers are relatively thicker at small scale. A scaling factor would be needed for transposition. It is also worth noting that the geometrical and loading conditions for flow separation could differ, depending on the Reynolds number. Therefore, the present observations refer to clearly established flow regimes that might be encountered for different loads and/or effective angles of attack at full scale. The effects of LE/TE devices are expected to be the same, at the condition that the flow regime is the same.

Bibliography

[1] F. Avallone, S. Pröbsting, and D. Ragni. Three-dimensional flow field over a trailing-edge serration and implications on broadband noise. *Physics of Fluids*, 28, 2016.

[2] F. Avallone, W.C.P. van der Velden, and D. Ragni. Benefits of curved serrations on broadband trailing-edge noise reduction. *J. Sound & Vib.*, 400:167–177, 2017.

[3] F. Avallone, W.C.P. van der Velden, D. Ragni, and D. Casalino. Noise reduction mechanisms of sawtooth and combed-sawtooth trailing-edge serrations. *J. Fluid Mech.*, 848:560–591, 2018.

[4] L.J. Ayton. Analytic solution for aerodynamic noise generated by plates with spanwise-varying trailing edges. *J. Fluid Mech.*, 849:448–466, 2018.

[5] L.J. Ayton and P. Chaitanya. An analytical and experimental investigation of aerofoil-turbulence interaction noise for plates with spanwise-varying leading edges. *J. Fluid Mech.*, 865:137–168, 2019.

[6] L.J. Ayton and N. Peake. On high-frequency sound generated by gust-aerofoil interaction in shear flow. *J. Fluid Mech.*, 766:297–325, 2015.

[7] G. Bampanis, M. Roger, and S. Moreau. On a three-dimensional investigation of airfoil turbulence-impingement noise and its reduction by leading-edge tubercles. *J. Sound & Vib.*, 520:116635, 1–18, 2022.

[8] P. Chaitanya, P. Joseph, S. Narayanan, C. Vanderwel, J. Turner, J.W. Kim, and B. Ganapathisubramani. Performance and mechanism of sinusoidal leading edge serrations for the reduction of turbulence-aerofoil interaction noise. *J. Fluid Mech.*, 818:435–464, 2017.

[9] B. Cotté and P. Blanc-Benon. Estimates of the relevant turbulent scales for acoustic propagation in an upward refracting atmosphere. *Acta Acustica un. Acustica*, 93(6):944–958, 2007.

[10] A. Finez, E. Jondeau, M. Roger, and M.C. Jacob. Broadband noise reduction of a linear cascade with trailing edge serrations. In *17th AIAA/CEAS Aeroacoustics Conference*, paper 2011-2874, Portland OR, 2011.

[11] F.E. Fish. Biomimetics: Determining engineering opportunities from nature. *Proc. SPIE - The International Society for Optical Engineering*, 2009.

[12] M. Gruber, P. Joseph, and T.P. Chong. Experimental investigation of airfoil self noise and turbulent wake reduction by the use of trailing edge serrations. In *16th AIAA/CEAS Aeroacoustics Conference*, paper 2010-3803, Stockholm, Sweden, 2010.

[13] S. Oerlemans, M. Fisher, T. Maeder, and K. Kögler. Reduction of wind turbine noise using optimized airfoils and trailing-edge serrations. *AIAA Journal*, 47(6):1470–1481, 2009.

[14] S. Oerlemans and B. Mendez-Lopez. Acoustic array measurements on a full scale wind turbine. In *11th AIAA/CEAS Aeroacoustics Conference*, paper 2005-2963, Monterey CA, 2005.

[15] C. Paruchuri, P. Joseph, S. Narayanan, C. Vanderwel, J. Turner, J.W. Kim, and B. Ganapathisubramani. Performance and mechanism of sinusoidal leading edge serrations for the reduction of turbulence-aerofoil interaction noise. *J. Fluid Mech.*, 818:435–464, 2017.

[16] C. Paruchuri, N. Subramanian, P. Joseph, C. Vanderwel, J.W. Kim, and B. Ganapathisubramani. Broadband noise reduction through leading edge serrations on realistic aerofoils. In *21st AIAA/CEAS Aeroacoustics Conference*, paper 2015-2202, Dallas, TX, 2015.

[17] M. Roger and S. Moreau. Extensions and limitations of analytical airfoil broadband noise models. *Int. J. of Aeroacoustics*, 9(3):273–305, 2010.

[18] H. Schlichting. *Boundary Layer Theory.* McGraw-Hill, 6th edition, 1968.

[19] Y. Wang, K. Zhao, X.Y. Lu, Y.B. Song, and G.J. Bennett. Bio-inspired aerodynamic noise control: A bibliographic review. *MDPI Appl. Sci.*, 9:2224, 2019.